Results in Physics 9 (2018) 682–691

Contents lists available at ScienceDirect

Results in Physics

journal homepage: www.journals.elsevier.com/results-in-physics

Rheological effects of micropolar slime on the gliding motility of bacteria with slip boundary condition

Z. Asghar [a,*], N. Ali [a], O. Anwar Bég [b], T. Javed [a]

[a] Department of Mathematics and Statistics, International Islamic University, Islamabad 44000, Pakistan
[b] Fluid Mechanics, Aeronautical and Mechanical Engineering Department, School of Computing, Science and Engineering (CSE), University of Salford, M54WT, UK

ARTICLE INFO

Article history:
Received 15 January 2018
Received in revised form 12 February 2018
Accepted 27 February 2018
Available online 8 March 2018

Keywords:
Gliding bacteria
Undulating surface model
Micropolar fluid
Slip effects
Exact solution
Modified Newton-Raphson method

ABSTRACT

Gliding bacteria are virtually everywhere. These organisms are phylogenetically diverse with their hundreds of types, different shapes and several modes of motility. One possible mode of gliding motility in the rod shaped bacteria is that they propel themselves by producing undulating waves in their body. Few bacteria glides near the solid surface over the slime without any aid of flagella so the classical Navier-Stokes equations are incapable of explaining the slime rheology at the microscopic level. Micropolar fluid dynamics however provides a solid framework for mimicking bacterial physical phenomena at both micro and nano-scales, and therefore we use the micropolar fluid to characterize the rheology of a thin layer of slime and its dominant microrotation effects. It is also assumed that there is a certain degree of slip between slime and bacterial undulating surface and also between slime and solid substrate. The flow equations are formulated under long wavelength and low Reynolds number assumptions. Exact expressions for stream function and pressure gradient are obtained. The speed of the gliding bacteria is numerically calculated by using a modified Newton-Raphson method. Slip effects and effects of non-Newtonian slime parameters on bacterial speed and power are also quantified. In addition, when the glider is fixed, the effects of slip and rheological properties of micropolar slime parameters on the velocity, microrotation (angular velocity) of spherical slime particles, pressure rise per wavelength, pumping and trapping phenomena are also shown graphically and discussed in detail. The study is relevant to emerging biofuel cell technologies and also bacterial biophysics.

Introduction

Prokaryotic microorganisms achieve locomotion by several possible modes, for instance, swimming in a fluid medium, crawling, gliding, and skimming over solid substrates. Among these microorganisms, *gliding* is adopted by rod-shaped bacteria which do not possess flagella. Some pertinent examples include flexibacter stain BH 3, cytophaga, oscillatoria and vitreoscilla. This gathering of life forms also incorporates the phototrophic cyanobacteria and a portion of the phototrophic green microbes and additionally the chemoheterotropic filamentous floating microscopic organisms, fruiting myxobacteria, and cytophagae. Generally, few of these bacteria glide on a thin layer of adhesive slime. The slime is basically a loose thin sheath, composed of exopolysaccharides, glycoproteins and glycolipids secreted by the bacterium, and is distinct to the *S-layer* (surface layer). The S-layer consist of monomolecular layer composed of (5 to 10% of total cell protein) glycoprotein. Bacterial S-layers (present in most of the gliding bacteria) plays an important role in enhancing their ability to associate with macrophages, shape maintenance of bacterium, molecular sieving and facilitating binding of bacterium to the host molecules [1]. The role of S-layer in bacterial motion is very important. S-layer helps to maintain overall rigidity of the cell wall and surface layers, as well as cell shape, which are important for self-propulsion. S-layers protect the cell from ion/pH changes, osmotic stress, detrimental enzymes, bacterial viruses, and predator bacteria. They can provide cell adhesion to other cells or surfaces. For pathogenic bacteria they can provide protection from phagocytosis.

Bacterial gliding is not only limited to aqueous phases but adjusted to drier regions and to development inside of solid masses, for example, soil, silt, and decaying wood that are penetrated by little channels [2]. The exact mechanism of gliding motility is still in debate. Available literature supports the bacterial motility by rotating cell surface discs, electro-kinesis, slime secretion, osmotic forces, generating peristaltic waves within their surface, and contractile components [3,4]. Here, we focus our attention in examining the bacterial gliding by means of *undulatory waves* in its outer surface. This approach has been supported by

* Corresponding author.
E-mail address: zee.qau5@gmail.com (Z. Asghar).

https://doi.org/10.1016/j.rinp.2018.02.070
2211-3797/

numerous researchers who have confirmed the robustness of the theory of bacterial gliding as a result of undulating waves in the external layer of their cell and due to the secretion of the parallel array of slime fibrils. This hypothesis was suggested by Costerton et al. [5] as a possible mechanism of gliding motility adopted by vitreoscilla. Halfen and Castenholz [6] suggested that gliding motility in blue-green algae (oscillatoria princeps) is due to its wavy surface, which is nearly in contact with the solid boundary.

Humphrey et al. [7] supported the hypothesis of flexibacter's movement by dispatching waves in its own outer surface. Read et al. [8] accepted this theory as a mechanism responsible for generating the necessary force for gliding in cyanobacteria. In his review article, Hoiczyk [9] reported on the generation of small surface waves, which travel down the filament surface, as one of the two possible mechanism adopted by cyanobacteria for motility. The micrographical results of the locomotion of cytophaga sp strain RB1058 also confirms the same phenomenon of gliding motility (associated with undulating outer surface) on a trail of thin liquid over a solid wall [10]. These biological studies motivated O'Brien [11] to develop a mathematical model to study the gliding motion of bacteria. He calculated the power dissipation and maximum speed of the flexibacter using lubrication theory. Subsequently the locomotion of the flexibacter by the same mechanism was addressed by Wakabayashi et al. [12] and later by Ridgway and Lewin [13]. Nakane et al. [14] observed a novel apparatus composed of Gld and Spr proteins for *Flavobacterium* gliding. In view of their results they proposed a model for *Flavobacterium* gliding supported by mathematical analysis. A focal adhesion-based mechanism in *Myxococcus xanthus* is thoroughly analyzed by Islam *and Mignot* [15]. The study carried out by McBride *and Nakane* [16] reveals that Flavobacterium johnsoniae glides due to motility adhesins SprB and RemA which are delivered to the cell surface type IX secretion system. Miyata *and Hamaguchi* [17] discussed the prospects for gliding of Mycoplasma mobile. In their viewpoint gliding machinery of this cell is composed of huge surface proteins and internal jellyfish-like structure. The gliding mechanisms reported in literature for myxobacteria, flavobacteria and mycoplasmas are recently discussed in an excellent review article by Nan and Zusman [18]. For myxobacteria they discussed two possible mechanisms of gliding out of which helical roter model is based on secretion of slime and generation of retrograde surface waves in the cell.

The slime secreted by the bacteria is quite complex and cannot be characterized by the Newtonian constitutive law [19–21]. Based on this observation, several *non-Newtonian* models have been deployed in bacterial hydrodynamic gliding studies. These include the third grade, power law, Johnson-Segalman and Carreau model which have been utilized by Siddiqui et al. [22], Hayat et al. [23], Wang et al. [24], Mahomed et al. [25] and Ali et al. [26], respectively. Most recently Asghar et al. [35] discussed the bacterial gliding motility by assuming three viscoelastic models namely FENE-P, SPTT and Rabinowitsch model simultaneously. In both studies [26,35], they used perturbative approach to calculate the gliding speed which is valid for small values of rheological parameters with no slip boundary condition. However, no study is available in the literature, in which the Eringen micropolar fluid model is integrated in the undulating surface models with slip effects to describe the non-Newtonian behavior of the slime. Micropolar fluids describe randomly oriented particles suspended in a viscous medium that represents the effects of microstructure.

The hypothesis of micropolar fluids was basically developed by Eringen [27,28]. The characteristics of micropolar fluids such as non-symmetric tensor, intrinsic motion and local microstructures makes them more sophisticated than other non-Newtonian fluid models. Due to these characteristics, micropolar fluid models have been extensively used to simulate complex phenomena in a diverse array of liquids including polymers, plastic sheets, ferrofluids, liquid crystals, biological fluids etc. Some applications of micropolar models in boundary layer flows, industrial flows, cavity flows, stretching sheet problems, blood flows, swimming problems etc. is documented in Refs. [29–32,37–47].

Most of the bacterial gliding studies were analyzed without considering the slip boundary condition. But, in real biological systems there is always a certain amount of slip and no-slip boundary condition is no longer valid as the bacteria secretes the slime and glides due to a negligible resistance and considerable slip effects between its lower surface and slime and also present between the slime and solid substrate. Considering such models along with slip effects at the wall (specially their dependence on shear stress) gives us more insight of the biophysical problem (see Refs. [32–34]). It is strongly anticipated that the glider's speed, forces produced by the glider and power (required for propulsion) will be significantly altered with the rheological parameters of the micropolar model and slip boundary condition at both ends. The choice of micropolar fluid with slip condition give us the exact solution for stream function and pressure gradient which is not the case in our previous studies [26,35] with no slip condition. This new finding helps us to calculate the gliding speed for large values of the rheological parameter. Moreover, in the present case the distance between bacterial lower surface and solid substrate is so small (filled with a thin layer of non-Newtonian fluid) which give rise to the dominant microrotation effects of the spherical slime particle.

The present letter is arranged as follows: In Section "Micropolar slime model and mathematical analysis", we present the geometry of the problem along with the governing equations for micropolar fluid which is used to simulate the bacterial slime. The problem is also formulated with *lubrication theory* i.e. long wavelength approximation and low Reynolds number assumptions in Sectio n "Micropolar slime model and mathematical analysis". Exact solutions are determined in Section "Exact solutions". In Section "Forces generated and power required for propulsion", the forces generated by the organism and power required for propulsion are presented. Gliding speed is calculated in Section "Gliding speed of the organism". The results obtained for a fixed glider are explained in Section "The pumping problem". Conclusions are summarized in Section "Conclusions". All the constants involved in the solution of the problem are listed in the Appendix.

Micropolar slime model and mathematical analysis

Let (U and V) are the velocity components along X- and Y-directions (i.e. fixed frame $OXYZ$), respectively. Fig. 1 illustrates the undulating surface model in which the upper peristaltic wall represents the rightward moving waves generated in the outer surface of the bacteria. The velocity of the wave is c. Due to these continuous moving waves bacteria pushes backward a thin layer of *micropolar slime* and thus, engaging itself in a self-powered motion called *gliding* that permits the organism to propel with speed V_g near the lower slippery solid boundary (substratum). So $(V_g - c)$ is the *relative* wave speed with respect to the fixed frame *(OXYZ)*. The profile of the sinusoidal wave within the glider's outer surface is described by the following expression [22–26].

$$h(X,t) = h_0 + a\,Sin\left[\left(\frac{2\pi}{\lambda}\right)(X - (c - V_g)t)\right], \tag{1}$$

where a is the amplitude, λ is the wavelength and h_0 is the mean distance of organism from the solid substrate. In the fixed frame, the flow is *unsteady*. However, it can be treated as *steady* in a frame *oxyz moving* with the speed c. The frame $oxyz$ is called the wave frame.

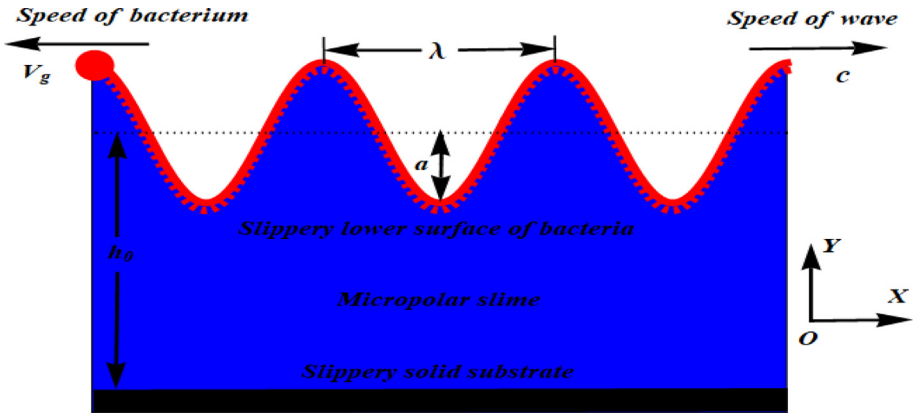

Fig. 1. Schematic diagram of two-dimensional undulating surface model.

The dimensional slip conditions in fixed frame (*OXYZ*) of reference are

$$U = -V_g - \frac{l}{\eta}T_{XY} \text{ at } Y = h,$$
$$U = \frac{l}{\eta}T_{XY} \text{ at } Y = 0, \tag{2}$$

where l is the slip length. The choice of slip condition is motivated by the fact that the slime beneath glider is typically a non-Newtonian fluid [26,35] and it is generally accepted that there is a certain amount of slip present when non-Newtonian fluids flow in contact to a solid boundary. This behavior of non-Newtonian fluid is quite different from Newtonian fluids for which adherence condition is valid. The transformations relating coordinates, velocities and pressures between the fixed frame (OXYZ) and the wave frame (oxyz) are defined as:

$$x = X - (c - V_g)t, \quad y = Y,$$
$$u = U - (c - V_g), \quad v = V, \quad P = p \tag{3}$$

where u, v are the respective velocity components in the wave frame along the x and y directions. The constitutive equations characterizing the steady flow of the micropolar slime in the wave frame are given by

$$v_{i,i} = 0, \tag{4}$$

$$\rho v_j v_{i,j} = T_{ij,j}, \tag{5}$$

$$\rho j v_j w_{i,j} = \Gamma_{ij,j} + \varepsilon_{ijk}T_{jk}, \tag{6}$$

while the linear constitutive laws take the forms [27,32].

$$T_{ij} = -p\delta_{ij} + \frac{1}{2}(2\eta + k)(v_{i,j} + v_{j,i}) + k\varepsilon_{ijk}(\omega_k - w_k), \tag{7}$$

$$\Gamma_{ij} = \alpha w_{k,k}\delta_{ij} + \beta w_{i,j} + \gamma w_{j,i}, \tag{8}$$

where T_{ij} and Γ_{ij} are Cauchy stress tensor and couple stress tensor, respectively. δ_{ij} is the Kronecker delta, ε_{ijk} is the alternating tensor, p is the isotropic pressure, v_i are the components of velocity vector, ω_i are the components of vorticity vector $(\omega_i = (1/2)\varepsilon_{ijk}v_{k,j})$ and w_i are the components of micro-rotation vector $\boldsymbol{w}$ and ρ and j are the fluid density and micro-gyration parameter and a comma after a suffix denotes covariant differentiation. Furthermore, the coefficients of viscosity η, k and the coefficients of gyroviscosity α_g, β_g and γ_g satisfy the following inequalities [27,32]:

$$2\eta + k \geqslant 0, \quad k \geqslant 0, \quad 3\alpha_g + \beta_g + \gamma_g \geqslant 0, \quad \gamma_g \geqslant |\beta_g|. \tag{9}$$

The choice of micropolar model for slime is driven by the fact that the gap between substrate and glider is very small (of the order 10^{-5} m). The micro-rotation effect is of crucial importance for flows in narrow gapes (channel). It is expected that when fluid flow through such gap the micro-rotation of the fluid particles (micropolarity of the fluid) affect the important flow characteristics. This factor is investigated thoroughly by Pietal [31] for squeeze flow of water, blood and electro-rheological suspension using micropolar fluid. In view of the above fact, it is quite natural to investigate the effect of micropolarity of the fluid on gliding mechanism.

The velocity field of the slime is given by $\boldsymbol{v} = (u, v, 0)$ and its particle's micro-rotation vector is $\boldsymbol{w} = (0, 0, w)$. To facilitate solutions, the following dimensionless variable and numbers are introduced:

$$x^* = \frac{2\pi}{\lambda}x, \quad y^* = \frac{y}{h_0}, \quad u^* = \frac{u}{c}, \quad v^* = \frac{v}{\delta c}, \quad h^* = \frac{h(x)}{h_0},$$
$$p^* = \frac{2\pi h_0^2}{\lambda\eta c}p, \quad T_{ij}^* = \frac{h_0}{\eta c}T_{ij}, \quad j^* = \frac{1}{h_0^2}j, \quad \delta = \frac{2\pi h_0}{\lambda}, \quad Re = \frac{\rho c h_0}{\eta},$$
$$N = \frac{k}{\eta + k}, \quad m = \sqrt{\frac{N(2-N)}{\varepsilon(1-N)}}, \quad \varepsilon = \frac{\gamma_g}{h_0^2\eta} \tag{10}$$

Further we define a stream function by the relations

$$u^* = \frac{\partial\psi}{\partial y^*}, \quad v^* = -\frac{\partial\psi}{\partial x^*}, \tag{11}$$

Substituting Eqs. (7) and (8) into Eqs. (4)–(6), using relations (10) the resulting dimensionless conservation equations for linear momentum and angular momentum (micro-rotation) emerge as:

$$\delta\, Re\left[\left(\frac{\partial\psi}{\partial y}\frac{\partial}{\partial x} - \frac{\partial\psi}{\partial x}\frac{\partial}{\partial y}\right)\left(\frac{\partial\psi}{\partial y}\right)\right] = -\frac{\partial p}{\partial x} + \frac{1}{1-N}\left[N\frac{\partial w}{\partial y} + \left(\delta^2\frac{\partial^2}{\partial x^2} + \frac{\partial^2}{\partial y^2}\right)\left(\frac{\partial\psi}{\partial y}\right)\right], \tag{12}$$

$$\delta^3\, Re\left[\left(\frac{\partial\psi}{\partial y}\frac{\partial}{\partial x} - \frac{\partial\psi}{\partial x}\frac{\partial}{\partial y}\right)\left(\frac{\partial\psi}{\partial x}\right)\right] = \frac{\partial p}{\partial y} + \frac{\delta^2}{1-N}\left[N\frac{\partial w}{\partial x} + \left(\delta^2\frac{\partial^2}{\partial x^2} + \frac{\partial^2}{\partial y^2}\right)\left(\frac{\partial\psi}{\partial x}\right)\right], \tag{13}$$

$$\frac{\delta j Re(1-N)}{N}\left[\left(\frac{\partial\psi}{\partial y}\frac{\partial}{\partial x} - \frac{\partial\psi}{\partial x}\frac{\partial}{\partial y}\right)w\right] = -2w + \left(\delta^2\frac{\partial^2}{\partial x^2} + \frac{\partial^2}{\partial y^2}\right)\left[\frac{\varepsilon(1-N)}{N}w - \psi\right]. \tag{14}$$

In the above equations, the superscript $*$ is omitted for the brevity. It is noted that due to the solenoidal nature of the microrotation vector, the coefficient of gyroviscosity α_g and β_g do not appear in the governing equations. Moreover, these equations reduce to the classical Navier-Stokes equations (for the Newtonian case) when N, ε and j vanish. Employing the long wavelength and low Reynolds number assumption, Eqs. (12)–(14) reduce to [22–26]:

$$\frac{\partial^3\psi}{\partial y^3} = (1-N)\frac{\partial p}{\partial x} - N\frac{\partial w}{\partial y}, \tag{15}$$

$$\frac{\partial p}{\partial y} = 0, \tag{16}$$

$$\frac{\varepsilon(1-N)}{N}\frac{\partial^2 w}{\partial y^2} - 2w = \frac{\partial^2\psi}{\partial y^2}. \tag{17}$$

Eqs. (15)–(17) are subject to following slip boundary conditions:

$$\begin{aligned} &\psi = 0, \quad \frac{\partial\psi}{\partial y} = V_b + \beta T_{xy}, \quad w = 0, \quad at\ y = 0,\\ &\psi = F, \quad \frac{\partial\psi}{\partial y} = -1 - \beta T_{xy}, \quad w = 0, \quad at\ y = h, \end{aligned} \tag{18}$$

where $\beta\left(=\frac{l}{h_0}\right)$ and $\phi\left(=\frac{a}{h_0}\right)$ is the slip and occlusion parameter, respectively with $V_b = \frac{V_g}{c} - 1$. Here the flow rates in fixed ($OXYZ$) and wave ($Oxyz$) frames are denoted by Θ and F, respectively. They are related to each other according to [26]:

$$\Theta = F - V_b. \tag{19}$$

Exact solutions

In view of Eq. (16), Eq. (15) can be written as:

$$\frac{\partial^3\psi}{\partial y^3} = \frac{\partial}{\partial y}\left[(1-N)\frac{dp}{dx}y - Nw\right]. \tag{20}$$

Integration of Eq. (20) yields:

$$\frac{\partial^2\psi}{\partial y^2} = (1-N)\frac{dp}{dx}y - Nw + C_1. \tag{21}$$

Using Eq. (21) in Eq. (17), we get

$$\frac{d^2w}{dy^2} - m^2 w = (1-N)\chi^2\frac{dp}{dx}y + \chi^2 C_1. \tag{22}$$

The general solution of Eq. (22) is:

$$w = C_2\cosh my + C_3\sinh my + \frac{\chi^2}{m^2}\left[(1-N)\frac{dp}{dx}y + C_1\right]. \tag{23}$$

Replacing the value of w in Eq. (21) and integrating twice gives:

$$\begin{aligned}\psi = {} & (1-N)\frac{dp}{dx}\left(1+\frac{N\chi^2}{m^2}\right)\frac{y^3}{6} + C_1\left(1+\frac{N\chi^2}{m^2}\right)\frac{y^2}{2}\\ & - \frac{NC_2}{m^2}\cosh my - \frac{NC_3}{m^2}\sinh my + C_4 y + C_5, \end{aligned} \tag{24}$$

in which C_{1-5} are constant of integration, $m = \sqrt{(2-N)}\chi$ and $\chi^2 = N/\varepsilon(1-N)$.

The constants C_{1-5} can be determine by using boundary conditions (18) and are given by:

The axial pressure gradient is given by:

$$\frac{dp}{dx} = \frac{3\sinh hm(2F+h-hV_b)}{h(N-1)(I_{23}+I_{24}\sinh hm)}. \tag{25}$$

For the micropolar slime, the stress tensor is non-symmetric. The dimensionless forms of the shear and normal stresses for the problem under consideration are given by:

$$T_{xy} = \frac{\partial^2\psi}{\partial y^2} - \left(\frac{N}{1-N}\right)w, \tag{26}$$

$$T_{yx} = \left(\frac{1}{1-N}\right)\frac{\partial^2\psi}{\partial y^2} + \left(\frac{N}{1-N}\right)w, \tag{27}$$

$$T_{xx} = 0, \quad T_{yy} = 0, \tag{28}$$

In view of Eq. (25), the dimensionless *pressure rise per wave length* is given by:

$$\Delta p_\lambda = \int_0^{2\pi}\frac{dp}{dx}dx = \int_0^{2\pi}\frac{3\sinh hm(2F+h-hV_b)}{h(N-1)(I_{23}+I_{24}\sinh hm)}dx. \tag{29}$$

Forces generated and power required for propulsion

The dimensionless horizontal and vertical forces on the bacterial organism surface are given by

$$F_x = \int_0^{2\pi}\tau_x|_{y=h}dx, \quad F_y = \int_0^{2\pi}\tau_y|_{y=h}dx, \tag{30}$$

Here τ_x and τ_y are components of the stress vectors $\boldsymbol{\tau}$ defined as follows:

$$\boldsymbol{\tau} = \begin{pmatrix}\tau_x\\ \tau_y\end{pmatrix} = \begin{pmatrix} p\frac{\partial h}{\partial x} + T_{xy}\\ -\frac{1}{\delta}p + T_{yy}\end{pmatrix}. \tag{31}$$

For brevity, here we omit the detailed derivation of Eq. (32), which can be found in Ref. [22]. From, Eqs. (26)–(28) and (31), Eq. (30) gives:

$$F_x = \int_0^{2\pi}\left(\frac{3\sinh hm(2F+h-hV_b)}{(1-N)(I_{23}+I_{24}\sinh hm)} + \frac{m(N-2)(I_{25}+\sinh hmI_{26})}{2I_{27}I_{28}}\right)dx, \tag{32}$$

$$F_y = 0. \tag{33}$$

The vertical force is zero, due to the choice of symmetric wave form on the glider surface. In the moving frame of reference this wave causes the glider surface to move to and fro in y-*direction*. Therefore the horizontal component of $\boldsymbol{\tau}$ does not play any role in the power propulsion. The power required for propulsion in non-dimensional form [11] is:

$$P = -\int_0^{2\pi} p\frac{dh}{dx}dx \tag{34}$$

Integration of (34) yields:

$$P = \int_0^{2\pi} h\frac{dp}{dx}dx = \int_0^{2\pi}\frac{3\sinh hm(2F+h-hV_b)}{(N-1)(I_{23}+I_{24}\sinh hm)}dx. \tag{35}$$

Gliding speed of the organism

Bacterium steadily glides over a solid wall only when the equilibrium condition (i.e. F_x, F_y and ΔP_λ must be zero) is satisfied. As in the Newtonian case, the lift force (F_y) generated by the micropolar slime is also zero. Therefore, we are left with two nonlinear equations as a result of equating to zero the expressions of Δp_λ and F_x. These equations are:

$$\Delta p_\lambda(V_b, F) = \int_0^{2\pi}\left(\frac{dp}{dx}(V_b, F; x)\right)_{y=h}dx = 0, \tag{36}$$

$$F_x(V_b, F) = \int_0^{2\pi}\left(\tau_{xy}(V_b, F; x) - h\frac{dp}{dx}(V_b, F; x)\right)_{y=h}dx = 0. \tag{37}$$

From (36) and (37), it is difficult to find the closed form expressions of V_b and F in term of other parameters. Hence, for the fixed values of ϕ, m, β and N, one can calculate the plausible numerical values of F and V_b using the modified Newton-Raphson method. The numerical solution obtained via this procedure must satisfy physically realistic conditions such that $-1 < V_b < 0$ and $F < 0$. To employ modified Newton-Raphson method, we set

$$\boldsymbol{r} = \begin{bmatrix} V_b \\ F \end{bmatrix} \quad \text{and} \quad \boldsymbol{\eta} = \begin{bmatrix} \Delta p_\lambda \\ F_x \end{bmatrix}. \tag{38}$$

Starting with some initial guess, the refined values of V_b and F can be obtained using the formula:

$$\boldsymbol{r}_{i+1} = \boldsymbol{r}_i - \frac{\boldsymbol{\eta}(\boldsymbol{r}_i)}{J(\boldsymbol{r}_i)}, \quad \text{where } i = 0, 1, 2 \ldots, \tag{39}$$

where the Jacobian matrix J is defined as:

$$J = \begin{bmatrix} \frac{\partial}{\partial V_b}(\Delta p_\lambda) & \frac{\partial}{\partial F}(\Delta p_\lambda) \\ \frac{\partial}{\partial V_b}(F_x) & \frac{\partial}{\partial F}(F_x) \end{bmatrix}, \tag{40}$$

The iteration procedure described above is implemented in the symbolic code Mathematica and results obtained are shown graphically in Figs. 2–4.

To develop a compatibility between the experimental values i.e. $h_0 = 0.025$ μm, $\lambda = 0.07$ μm, $a = 0.015$ μm, $\eta = 1P$ and $V_g = 1.5$ μm/s (gliding speed of Flexibactar sp. Strain BH3) and our theoretical results Fig. 2 is plotted where, the value of wave speed can be approximated as $c = 2.5$ μm/s (see Refs. [22,35]). Hence the non-dimensional gliding speed can be approximated as $V_g/c = 0.6$.

Fig. 2 clearly testifies our model as it indicates that the plot reaches the experimental value of the bacterial speed with considerable slip effects.

In order to illustrate the general trend, gliding speed of the bacterium as a function of micropolar parameter (ε) is displayed in Fig. 3(a) for different values of slip parameter (β).

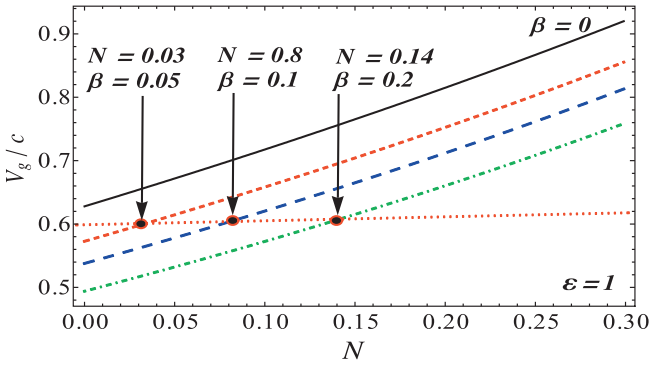

Fig. 2. Plot of non-dimensional gliding speed as a function of N.

This figure reveals the asymptotic behavior of the bacterial velocity profile for the large values of ε. It is revealed that for fixed occlusion ratio (ϕ) and coupling number (N), the organism achieves maximum velocity at $\varepsilon = 0.1$. Fig. 3(a) also reveals that the presence of slip (between bacterium and slime along with the slime and solid substrate) tends to slow down the gliding speed. The bacterial speed as a function of coupling number is depicted in Fig. 3(b) for different values of ϕ. It is observed that bacteria glides *faster* over a slime with large coupling numbers as compared to the slime for which $N = 0$ (Newtonian case). More efficient bacterial propulsion is therefore achieved in micropolar slime rather than Newtonian slime. Rheology of the bacterium environment therefore contributes to improving propulsive efficiency. Newtonian models under-predict the propulsive performance. The plot also confirms that the organism achieves more speed as the amplitude of wave with its outer surface gets larger.

Our results also estimate the power required for 0.5 μm wide and 10 μm long glider as 5.54×10^{-10} erg/s. Humphrey and Marshall [7] also reported the experimental value of power required to sustain such motion given as 5×10^{-7} erg/s. Our calculated value is much less than the experimental value given by Humphrey and Marshall, which confirms the feasibility of our analysis.

The variation in power propulsion is depicted in Fig. 4(a) and (b). Fig. 4(a) is in correspondence with Fig. 3(a). It is noted that power required for propulsion decreases in magnitude with increasing slip effects.

The power increases initially with increasing values of ε and for large values of ε it (power) exhibit asymptotic behavior. While Fig. 4(b) (is in correspondence with Fig. 3(b)) shows that the larger amplitude waves therefore necessitate greater power for propelling the bacterium. Moreover, a slight increase in power is also noted when slime rheology changes from Newtonian to micropolar.

The pumping problem

The closed form solution of Eqs. (15) and (17) along with the boundary conditions given in Eq. (18) is obtained and the influence of coupling number (N), micropolar parameter (ε), slip parameter (β), flux rate (F) and bacteria wave amplitude (ϕ) on velocity component (u) microrotation (w), pressure rise (Δp) and stream function (ψ) are graphically shown in Figs. 5–9 for $V_b = -1$. The case $V_b = -1$ corresponds to *the pumping scenario*, in which bacterium is stationary i.e., $V_g = 0$. Indeed, this case represents the *peristaltic flow of micropolar fluid between a substrate and a wavy wall.*

Fig. 5(a) and (b) have been plotted to illustrate the slip effects at two different flow rates along with the effects of micropolar parameter and coupling number on the velocity profile respectively. Both figures show parabolic velocity profiles indicating non-

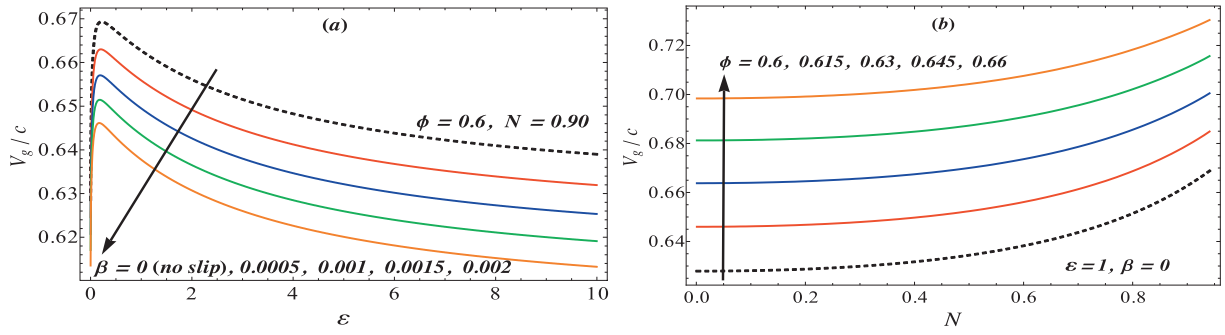

Fig. 3. Variation of the gliding speed with respect to the different rheological parameter.

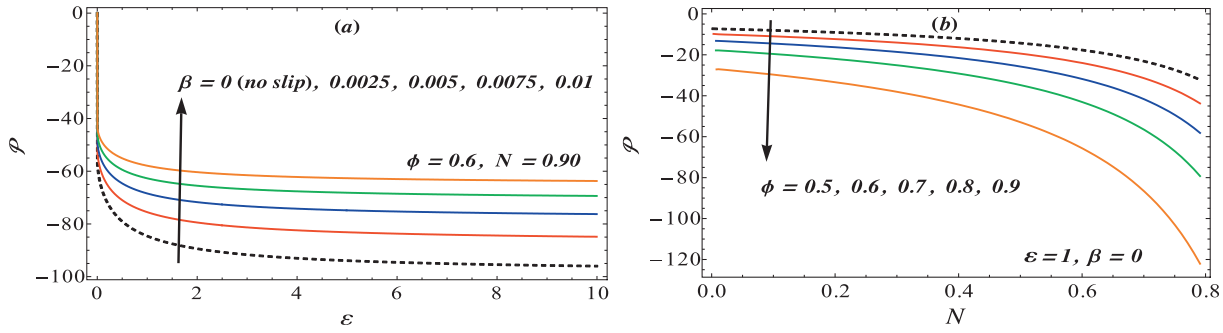

Fig. 4. Variation of power propulsion with respect to the different rheological parameter.

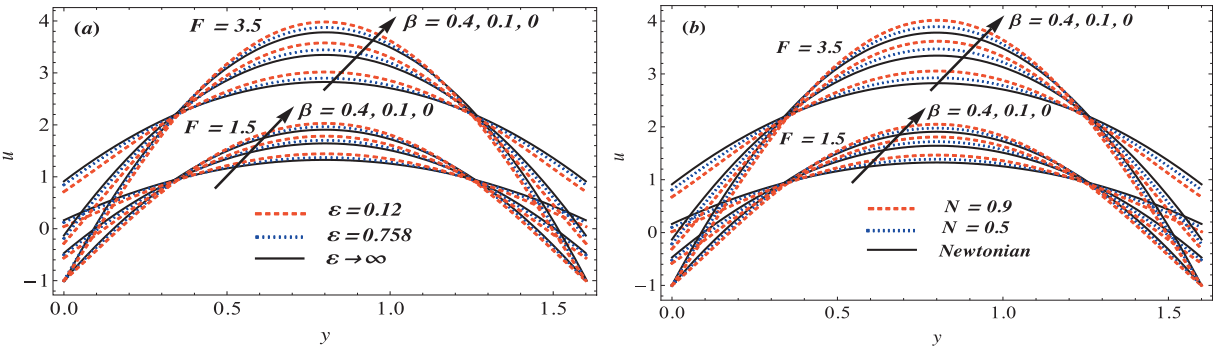

Fig. 5. Variation of velocity profile with respect to the different rheological parameter. Panel (a) $N = 0.8$ and panel (b) $\varepsilon = 4.8$, with $\phi = 0.6$ and $V_b = -1$.

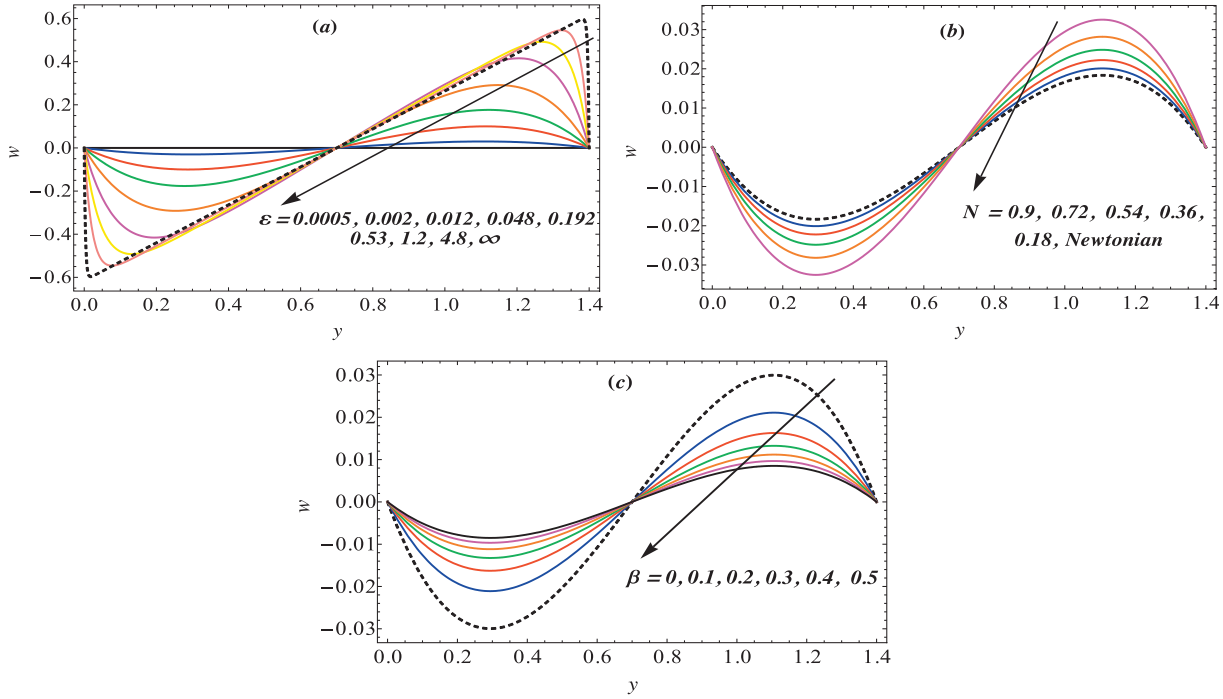

Fig. 6. Variation of microrotation profile with respect to the different rheological parameter with $\phi = 0.4$ and $V_b = -1$. Panel (a) $N = 0.8$, $\beta = 0$ and $F = -1$, panel (b) $\varepsilon = 4.8$, $\beta = 0$ and $F = -1$, and panel (c) $F = -1, N = 0.8$ and $\varepsilon = 4.8$.

linear velocity variations at the cross-section $x = -\pi/2$. It is further observed that with increasing the coupling number (N) or decreasing the micropolar parameter (ε), the slime velocity is increased (i.e. slime acceleration occurs) in the central part of the domain $y \in [0, h]$ while the opposite trend prevails in the vicinity of the walls. Fig. 5 also depicts that the slippery boundaries assist the flow of slime adjacent to it and as the distance from these slippery boundaries are increased (i.e. in the central part) the situation become opposite.

Fig. 6(a)–(d) illustrate the influence of micropolar parameter (ε), coupling number (N), flow rate (F) and slip parameter (β) on the microrotation of the spherical slime particles. It is clear from

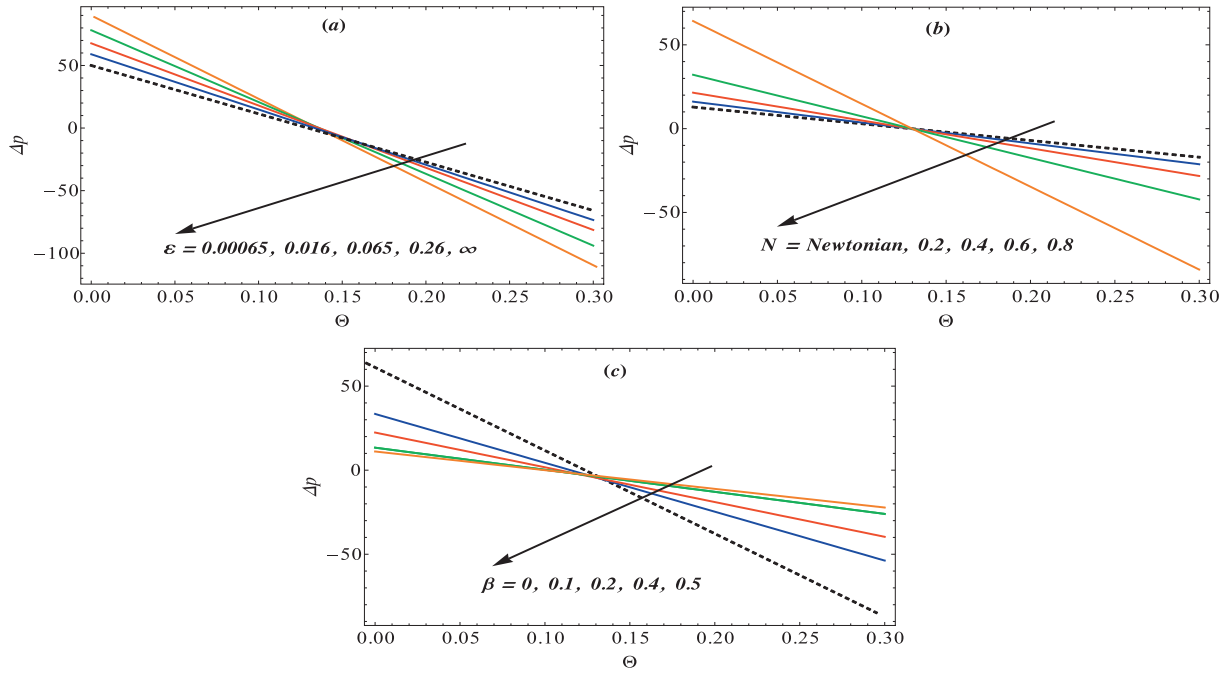

Fig. 7. Plots of pressure rise per wavelength Δp versus flow rate Θ for various values of ε, N, β and ϕ. Panel (a) $\phi = 0.3$, $\beta = 0$ and $N = 0.85$, panel (b) $\phi = 0.3$, $\beta = 0$ and $\varepsilon = 4.8$ and panel (c) $\phi = 0.3$, $N = 0.85$ and $\varepsilon = 4.8$. Here $V_b = -1$.

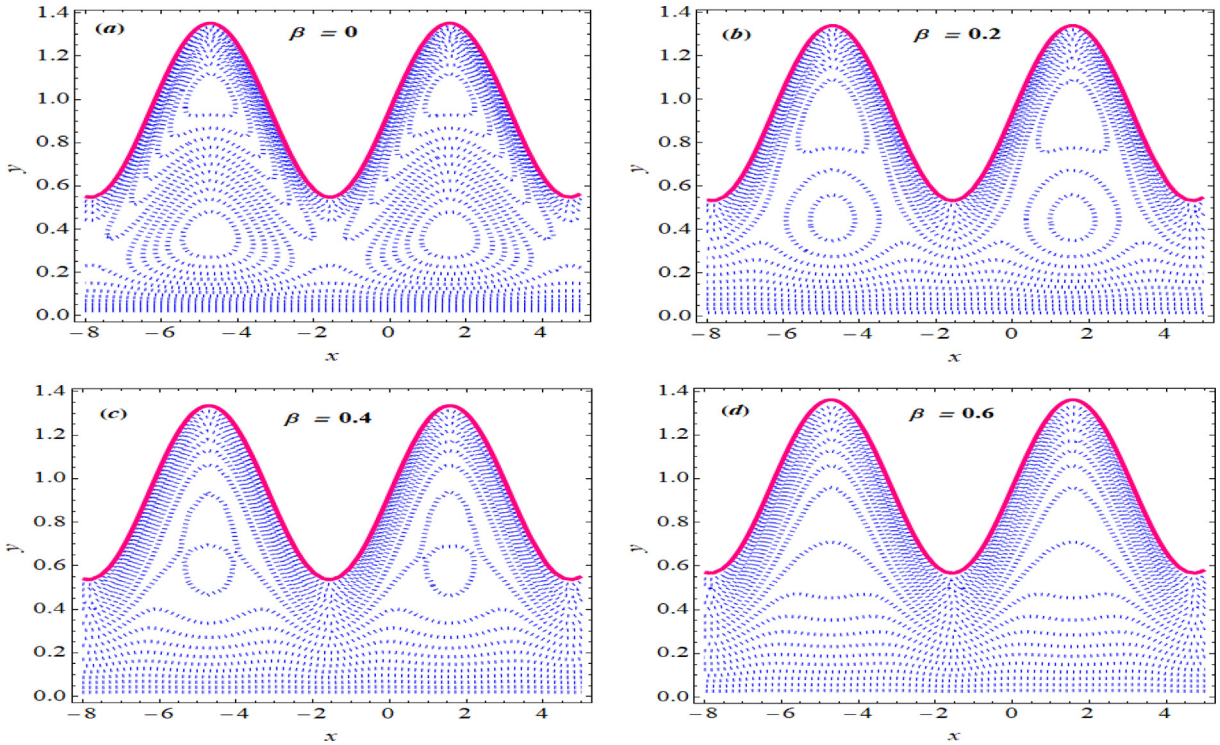

Fig. 8. The pattern of streamline for different values of β when $\phi = 0.4$, $N = 0.8$, $F = -0.2$, $V_b = -1$ and $\varepsilon = 4.8$.

Fig. 6 that the behavior of microrotation is symmetric about the center of the channel. The micro-rotation increases uniformly in magnitude with decreasing ε in both channel halves (Fig. 6(a)). For small values of ε, microrotation varies sharply near the walls and behaves linearly over the remainder of the cross section. This clearly indicates the formation of a thin boundary layer at both the walls for small values of ε.

In fact, in such case the micro elements of the slime exhibit strong rotation near the walls. In contrast, no such boundary layer is formed with increasing N and β although the microrotation increases in magnitude in both the channel halves with increasing N (Fig. 6(b)). In contrast Fig. 6(c) shows that the increase in the slip effects causes a reduction in the microrotation of the spherical slime particles.

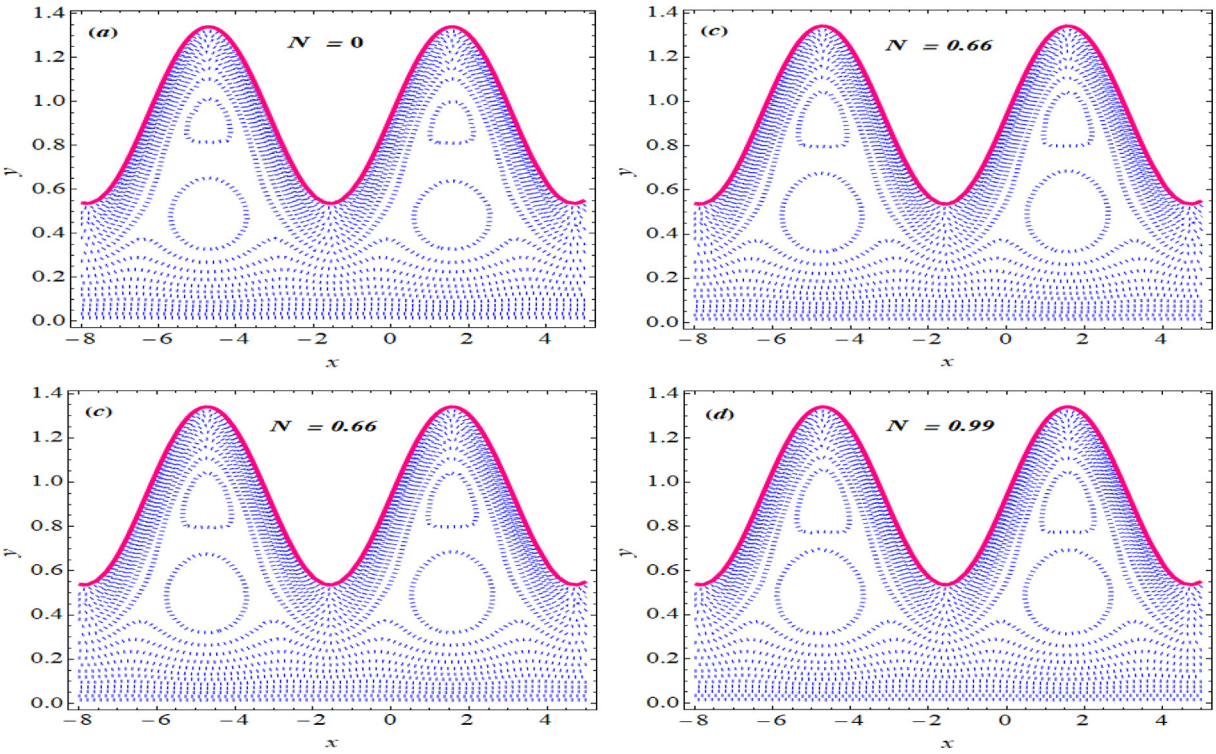

Fig. 9. The pattern of streamlines for different values of N when $\phi = 0.4$, $\beta = 0.25$, $F = -0.2$, $V_b = -1$ and $\varepsilon = 4.8$.

The plots of pressure rise per wavelength against time average flux Θ for different values of rheological parameters and slip parameter is illustrated in Fig. 7(a)–(c). It is demonstrated in Fig. 7(a) that pressure rise decreases in the pumping region $(\Delta p > 0, \Theta > 0)$ with decreasing micropolar parameter (ε). The free pumping flux i.e., Θ for $\Delta p = 0$ is found to decrease with increasing m. In the co-pumping region $(\Delta p < 0, \Theta > 0)$, the magnitude of pressure rise per wavelength decreases by reducing the values of ε.

Fig. 7(b) illustrates the effect of coupling number N on Δp. In the pumping region, larger values of coupling number (N), enhance the magnitude of Δp indicating that greater effort is rendered by the wavy wall (organism) to maintain the prescribed flux of a micropolar slime in comparison to the Newtonian slime scenario. The free pumping flux is nearly independent of the coupling parameter N. However, larger values of N in the co-pumping region enhance the magnitude of Δp. Fig. 7(c) shows a decrease in Δp with increasing β. Free pumping flux also decreases with increasing slip effects between the fixed glider and secreted slime and also between the moving slime and fixed substrate.

Fig. 8 displays the streamlines representing the slime flow pattern for four different values of the coupling number β. In general, it is noted that the streamlines resemble in shape the wavy wall boundary (shown with solid pink wave). However, some recirculating zones can be identified in the central region of the flow domain. These recirculating zones are largely dependent on the values of the involved parameters. Flow patterns of the slime for four different values of slip parameter are represented in Fig. 8. It is evident that the size of circulating bolus decreases with increasing β. Finally the bolus disappear at a particular value of slip parameter $\beta = 0.6$ as shown in Fig. 8. Finally, the streamlines patterns for different coupling numbers are shown in Fig. 9. The size of trapped bolus is enhanced with increasing coupling number. This further confirms that greater mixing is realized with increasing micropolarity of the slime.

Conclusions

The gliding motility of bacteria on a thin layer of micropolar slime is investigated employing an undulating surface model. The lubrication approximation theory (LAT) is utilized to simplify the flow equations of micropolar slime. The problem is solved analytically. The exact expression for the stream function ψ and pressure gradient dp/dx are also obtained. The Modified Newton Raphson method is used to calculate steady gliding speed of the organism. The pumping problem is also considered when the bacterium is held fixed and the associated undulating motion generates a net flow in the positive x-direction. Velocity, micro-rotation, pressure rise and streamlines for different values of rheological parameters are also plotted to observe the slime behavior. The principal observations from the current study can be summarized as:

- The bacterium glides faster on the micropolar slime as compared to the Newtonian slime.
- The speed of the organism increases with increasing amplitude of the undulating wave on the organism surface, while slip resist the gliding motility.
- The glider achieves maximum speed at $\varepsilon = 0.1$ irrespective of the choice of other parameters. These results are appropriate to use in Bio-mechatronics engineering to adjust the slime rheology with certain amount of slip in such a way that an artificial mechanical glider can attain its maximum speed.
- The gliding speed and power propulsion achieves asymptotic behaviors for large values of rheological parameters. These new results are quite interesting and give us more insight

to bacterial hydrodynamics, since our previous study [26,35] predicts the monotonic behavior for gliding speed and power at small values of rheological parameters.

- For the case when the organism is held fixed and its undulating motion generate a net flow in the positive x-direction, velocity of the slime follows an increasing trend at the channel center with increasing N (or decreasing ε).
- The microrotation profile is symmetric about the center of the channel and slime micro-elements rotate with the greater speed as the coupling number and micropolar parameter are increased but increasing slip result in reduction of microrotation of the slime particles.
- The pressure rise per wavelength in the pumping region increases with a departure in the slime rheology from Newtonian to micropolar.
- A modification in the slip parameter from 0 to 0.6 results in reduction of circulating zones and finally disappearance of the circulating bolus, while an opposite trend is observed with increasing coupling number.

Appendix

The constant involved in the solution of the problem are as follows

$$C_1 = \frac{I_6 + I_7 + I_8 V_b}{I_9 I_{10}}, \quad C_2 = I_2 C_1,$$

$$C_3 = I_2 C_1(\operatorname{csch} hm - \coth hm) + hI_2 \frac{dp}{dx}(1-N)\operatorname{csch} hm,$$

$$C_4 = \frac{I_{11}I_{12} - I_{13} + (I_{14}\beta - I_2 I_5 m I_{15}\operatorname{csch} hm)V_b}{I_{16} I_{17}},$$

$$C_5 = \frac{I_2 I_5 (I_{18} + 3I_2 I_5 m I_{19} + I_{20} V_b)}{I_{21} I_{22}},$$

$$I_1 = \frac{\chi^2}{m^2}(1-N), \quad I_2 = \frac{\chi^2}{m^2}, \quad I_3 = \frac{(1-N)}{6}\left(1 + N\frac{\chi^2}{m^2}\right)$$

$$I_4 = \frac{1}{2}\left(1 + N\frac{\chi^2}{m^2}\right), \quad I_5 = \frac{N}{m^2},$$

$$I_6 = h(3F+h)I_4 - 3I_4 I_5 + 3F(2I_4 - I_2 I_5 m^2)\beta,$$

$$I_7 = 3I_2 I_5 m(-F\coth hm + (F+h)\operatorname{csch} hm),$$

$$I_8 = -3I_2 I_5 + h(-2hI_4 - 6I_4\beta + 3I_2 I_5 m^2\beta) + 3hI_2 I_5 m\coth hm,$$

$$I_9 = 6I_2 I_5 + h(hI_4 + 6I_4\beta - 3I_2 I_5 m^2\beta) - 3hI_2 I_5 m\coth\frac{hm}{2},$$

$$I_{10} = hI_4 + 2I_4\beta - I_2 I_5 m^2\beta - I_2 I_5 m\tanh\frac{hm}{2},$$

$$I_{11} = 2I_4\beta - I_2 I_5 m^2\beta - I_2 I_5 m\coth hm,$$

$$I_{12} = h(3F+h)I_4 - 3I_2 I_5 + 3F(2I_4 - I_2 I_5 m^2)\beta - 3FI_2 I_5 m\coth hm,$$

$$I_{13} = I_2 I_5(h(3F+2h)I_4 + 3I_2 I_5)m\operatorname{csch} hm - 3F(I_2 I_5)^2 m^2(\operatorname{csch} hm)^2,$$

$$I_{14} = hI_4(h^2 I_4 + 6I_2 I_5) + (2h^2 I_4 + 3I_2 I_5)(2I_4 - I_2 I_5 m^2),$$

$$I_{15} = h^2 I_4 - 3I_2 I_5 + (2h^2 I_4 + 3I_2 I_5)\cosh hm,$$

$$I_{16} = 6I_2 I_5 + h(hI_4 + 6I_4\beta - 3I_2 I_5 m^2\beta) - 3hI_2 I_5 m\coth\frac{hm}{2},$$

$$I_{17} = hI_4 + 2I_4\beta - I_2 I_5 m^2\beta - I_2 I_5 m\tanh\frac{hm}{2},$$

$$I_{18} = h(3F+h)I_4 - 3I_2 I_5 + 3F(2I_4 - I_2 I_5 m^2)\beta,$$

$$I_{19} = -F\coth hm + (F+h)\operatorname{csch} hm,$$

$$I_{20} = -3I_2 I_5 + h(-2hI_4 - 6I_4\beta + 3I_2 I_5 m^2\beta) + 3hI_2 I_5 m\coth hm,$$

$$I_{21} = 6I_2 I_5 + h(hI_4 + 6I_4\beta - 3I_2 I_5 m^2\beta) - 3hI_2 I_5 m\coth\frac{hm}{2},$$

$$I_{22} = hI_4 + 2I_4\beta - I_2 I_5 m^2\beta - I_2 I_5 m\tanh\frac{hm}{2},$$

$$I_{23} = -3hI_2 I_5 m(1+\cosh hm),$$

$$I_{24} = 6I_2 I_5 + h(hI_4 + 6I_4\beta - 3I_2 I_5 m^2\beta),$$

$$I_{25} = -3(F+h)mN\cosh hm + 3mN(F - hV_b),$$

$$I_{26} = 3M + m^2(h(3F+2h) - 3(F+h)(-2+M)\beta) + (-h^2 m^2 + 3M)V_b,$$

$$I_{27} = 2m(h - (-2+N)\beta)\cosh\frac{hm}{2} - N\sinh\frac{hm}{2},$$

$$I_{28} = -3hmN\cosh\frac{hm}{2} + (6N + hm^2(h - 3(-2+M)\beta))\sinh\frac{hm}{2}.$$

References

[1] Mesnage S, Couture ET, Gounon P, Mock M, Fouet A. The capsule and S-layer: two independent and yet compatible macromolecular structures in Bacillus anthracis. J Bacteriol 1998;180:52–8.
[2] Kaiser D. Bacterial motility: how do pili pull? Curr Biol 2000;10:777–80.
[3] Koch AL. The sacculus contraction/expansion model for gliding motility. J Theor Biol 1990;142:95–112.
[4] Lapidus IR, Berg HC. Gliding motility of Cytophaga sp. strain U67. J Bacteriol 1982;151:384–98.
[5] Costerton JW, Murray RGE, Rabino CF. Observations on the motility and the structure of vitreoscilla. Can J Microbiol 1961;7:329–39.
[6] Halfen LN, Castenholz RW. Gliding in the blue-green alga: a possible mechanism. Nature 1970;225:1163–5.
[7] Humphrey BA, Dickson MR, Marshall KC. Physicochemical and in situ observations on the adhesion of gliding bacteria to surfaces. Arch. Microbiol. 1979;120:231–8.
[8] Read N, Connell S, Adams DG. Nanoscale visualization of a fibrillar array in the cell wall of Filamentous Cyanobacteria and its implications for gliding motility. J Bacteriol 2007;189:7361–6.
[9] Hoiczyk E. Gliding motility in cyanobacteria: observations and possible explanations. Arch Microbiol 2000;174:11–7.
[10] Burchard AC, Burchard RP, Kloetzel JA. Intracellular, periodic structures in the gliding bacterium Myxococcus Xanthus. J Bacteriol 1977;132:666–72.
[11] O'Brien RW. The gliding motion of a bacterium, Flexibactor strain BH 3. J Aust Math Soc (Ser B) 1981;23:2–16.
[12] Wakabayashi H, Hikida M, Masumura K. Flexibacter maritimus sp. nov., a Pathogen of Marine Fishes. IJSEM 1986;36:39.
[13] Ridgway HF, Lewin RA. Characterization of gliding motility in Flexibacter polymorphus. Cell Motil Cytoskeleton 1988;11:46–63.
[14] Nakane D, Sato K, Wada H, McBride MJ, Nakayama K. Helical flow of surface protein required for bacterial gliding motility. Proc Natl Acad Sci USA 2013;110:11145–50.
[15] Islam ST, Mignot T. The mysterious nature of bacterial surface (gliding) motility: a focal adhesion-based mechanism in *Myxococcus xanthus* Semin. Cell Dev Biol 2015;46:143–54.
[16] McBride MJ, Nakane D. Flavobacterium gliding motility and the type IX secretion system. Curr Opin Microbiol 2015;28:72–7.
[17] Miyata M, Hamaguchi T. Prospects for the gliding mechanism of Mycoplasma mobile. Curr Opin Microbiol 2016;29:15–21.
[18] Nan B, Zusman DR. Novel mechanisms power bacterial gliding motility. Mol Microbiol 2016;101:186–93.
[19] Christensen PJ. The history, biology and taxonomy of the Cytophaga group. Can J Microbiol 1977;23:1599–653.
[20] Sutherland IW. Polysaccharides produced by Cystobacter, Archangium, Sorangium and Stigmatella species. J Gen Microbiol 1979;111:211–6.
[21] Sutherland IW. Microbial exopolysaccharides-their role in microbial adhesion in aqueous systems. Crit Rev Microbiol 1984;10:173–202.
[22] Siddiqui AM, Burchard RP, Schwarz WH. An undulating surface model for the motility of bacteria gliding on a layer of non-Newtonian slime. Int J Non-Linear Mech 2001;36:743–61.
[23] Hayat T, Wang Y, Siddiqui AM, Asghar S. A mathematical model for the study of gliding motion of bacteria on a layer of non–Newtonian slime. Math Methods Appl Sci 2004;27:1447–68.
[24] Wang Y, Hayat T, Siddiqui AM. Gliding motion of bacteria on a power–law slime. Math Methods Appl Sci 2005;28:329–47.
[25] Mahomed FM, Hayat T, Momoniat E, Asghar S. Gliding motion of bacterium in a non-Newtonian slime. Nonlinear Anal Real World Appl 2007;8:853–64.
[26] Ali N, Asghar Z, Anwar Beg O, Sajid M. Bacterial gliding fluid dynamics on a layer of non-Newtonian slime: perturbation and numerical study. J Theor Biol 2016;397:22–32.
[27] Eringen AC. Theory of micropolar fluids. J Math Mech 1966;16:1–16.
[28] Eringen AC. Theory of thermomicrpolar fluids. J Math Anal Appl 1972;38:480–96.
[29] Philip D, Chandra P. Self-propulsion of spermatozoa in microcontinua: effect of trasverse wave motion of channel walls. Arch Appl Mech 1995;66:90–9.
[30] Sinha P, Singh C, Prasad KR. A micro-continuum analysis of the self-propulsion of the spermatozoa in the cervical canal. IJEST 1982;20:1037–48.

[31] Ishak A, Nazar R, Pop I. Flow of a micropolar fluid on a continuous moving surface. Arch Mech 2006;56:529–41.
[32] Rao IJ, Rajagopal KR. The effect of the slip boundary condition on the flow of fluids in a channel. Acta Mech 1999;135:113–26.
[33] Kwang W, Chu H, Fang J. Peristaltic transport in a slip flow. Euro Phys J B 2000;16:543–7.
[34] Ali N, Hussain Q, Hayat T, Asghar S. Slip effects on the peristaltic transport of MHD fluid with variable viscosity. Phys Lett A 2008;372:1477–89.
[35] Asghar Z, Ali N, Sajid M. Interaction of gliding motion of bacteria with rheological properties of the slime. Math Biosci 2017;290:31–40.
[37] Ijaz S, Nadeem S. Slip examination on the wall of tapered stenosed artery with emerging application of nanoparticles. Int J Therm Sci 2016;109:401–12.
[38] Nadeem S, Ijaz S. Theoretical examination of nanoparticles as a drug carrier with slip effects on the wall of stenosed arteries. Int J Heat Mass Transfer 2016;93:1137–49.
[39] Ijaz S, Nadeem S. Examination of nanoparticles as a drug carrier on blood flow through catheterized composite stenosed artery with permeable walls. Comput Methods Programs Biomed 2016;133:83–94.
[40] Ijaz S, Nadeem S. Biomedical theoretical investigation of blood mediated nanoparticles (Ag and Al_2O_3-blood) impact on hemodynamics of overlapped stenotic artery, Journal of molecular liquid. J Mol Liq 2017;248:809–21.
[41] Ijaz S, Shahzadi I, Nadeem S, Saleem A. A clot model examination: with impulsion of nanoparticles under the influence of variable viscosity and slip effects. Commun Theor Phys 2017;68. 676(5).
[42] Nazeer M, Ali N, Javed T. Numerical simulation of MHD flow of micropolar fluid inside a porous inclined cavity with uniform/non-uniform heated bottom wall. Can J Phys 2017. https://doi.org/10.1139/cjp-2017-0639.
[43] Ali N, Nazeer Mubbashar, Javed T, Siddiqui Muhammad Arshad. Buoyancy driven cavity flow of a micropolar fluid with variably heated bottom wall. Heat Trans Res 2018. https://doi.org/10.1615/HeatTransRes.2018019422.
[44] Ali N, Nazeer F, Nazeer Mubbashar. Flow and heat transfer analysis of Eyring-powell fluid in a pipe. ZNA 2018. https://doi.org/10.1515/zna-2017-0435.
[45] Nazeer Mubbashar, Ali N, Javed T. Effects of moving wall on the flow of micropolar fluid inside a right angle triangular cavity. Int J Numer Method H 2018. https://doi.org/10.1108/HFF-10-2017-0424.
[46] Waqas M, Farooq M, Khan MI, Alsaedi A, Yasmeen T. Magnetohydrodynamic (MHD) mixed convection flow of micropolar liquid due to nonlinear stretched sheet with convective condition. Int J Heat Mass Transfer 2016;102:766–72.
[47] Shehzad SA, Waqas M, Alsaedi A, Hayat T. Flow and heat transfer over an unsteady stretching sheet in a micropolar fluid with convective boundary condition. J Appl Fluid Mech 2016;9:1437–45.

Further reading

[36] Kucaba-Pietal A. Scale effect in microflows modeling with the micropolar theory. VIIEuropean congress on computational methods in applied sciences and engineering M, 2016.
[48] Zubair M, Waqas M, Hayat T, Ayub M, Alsaedi A. The onset of modified Fourier and Fick's theories in temperature-dependent conductivity flow of micropolar liquid. Results Phys 2017;7:3145–52.